Magnesiothermic Reduction of Thin Films: Towards Semiconducting Chiral Nematic Mesoporous Silicon Carbide and Silicon Structures

*Thanh-Dinh Nguyen, Joel A. Kelly, Wadood Y. Hamad, and Mark J. MacLachlan**

There is a growing demand for new methods to prepare porous Si-based materials for applications in optoelectronic and microelectronic devices. In this work, the preparation of SiC and Si from magnesiothermic reduction of chiral nematic SiO_2/C composites and mesoporous SiO_2, respectively, is reported. The SiO_2/C composites are prepared by cocondensing SiO_2 with cellulose nanocrystals (CNCs) followed by pyrolysis. The magnesiothermic reduction of the composites produces SiC after prolonged solid-state reaction, with mixed MgC_2/SiC intermediates. Iridescent mesoporous tetragonal MgC_2/SiC structures that retain the long-range twisted organization of the starting composites transform to mesoporous cubic SiC with a chiral nematic hierarchical structure, but with some loss of order. On the other hand, the magnesiothermic reduction of the chiral nematic mesoporous SiO_2 templated from CNCs affords mesoporous Si materials with a layered hierarchical structure. The structural properties and the conductivity of the products, as well as the reaction pathways by analysis of the materials at intermediate stages, are investigated. These experimental results show that the magnesiothermic reduction is a promising way to obtain new porous semiconducting materials with chiral nematic structures.

1. Introduction

Porous semiconducting materials such as ordered mesoporous structures,[1a] aerogels,[1b] anodically etched porous films,[1c] and inverse opals[1d] are of interest for numerous applications owing to their combination of high surface areas with size-dependent optoelectronic and thermal properties. Of particular interest is the family of group 14-based porous semiconductors (e.g., Si, SiC, Ge, Si_xGe_{1-x}, etc.), due to compatibility with the Si microfabrication industry[2] and concerns over toxicity of other II–VI and III–V semiconducting materials.[3] A major thrust in this area has been the incorporation of Si-based semiconductors into photonic structures such as inverse opals for integration into optical computing.[4] This is generally accomplished by chemical vapor deposition (CVD) of a suitable precursor (e.g., silylene–acetylene for SiC;[5a] disilane for Si)[5b] inside voids of a preassembled structure (e.g., an fcc array of silica or latex particles) and subsequent removal of the template. As a result, this approach is typically limited to the preparation of macroporous semiconductors to facilitate homogeneous diffusion and deposition of the precursor.

An alternative bottom-up approach for the preparation of group 14-based porous semiconductors is magnesiothermic reduction, first demonstrated by Bao *et al.*[6] for Si materials. By exploiting the low temperature of Mg vaporization to reduce the corresponding porous oxide precursor at 650–800 °C under inert atmosphere, this approach has been shown to preserve the shape of a variety of porous structures, including opals,[7a] ordered mesoporous films,[7b] or some naturally derived oxides such as silica-rich frustules,[6,7c] rice husks,[7d] and sand.[7e] Accordingly, porous Si replicas can be created through reduction of silica,[6] while porous SiC materials have been reported through the reduction of silica in the presence of carbon.[8] The magnesiothermic reduction process is carried out at substantially lower temperature than conventional methods (such as polycarbosilane pyrolysis for porous SiC at ≈1400 °C)[9] and requires minimal infrastructure available in most chemistry laboratories.

Several research groups have noted that the magnesiothermic reduction of silica can produce a mixture including Si, Mg_2Si, MgO, and unreacted SiO_2 through inhomogeneity introduced during the vapor transport process, depending on the distance between magnesium vapor source and silica substrate.[6,7] Additionally, Dasog et al.[10] have shown evidence for the formation of magnesium sesquicarbide (Mg_2C_3) as an intermediate in the magnesiothermic reduction of silica in the presence of carbon to form SiC. It is challenging to predict if a given porous precursor will retain its morphology through the transformation process as the reduction process can generate a multitude of by-products depending on the precursor composition and the experimental set up.

Chiral nematic liquid crystals (LCs) exhibit photonic properties when their helical pitch is on the order of the wavelengths of visible light, resulting in selective reflection of circularly polarized light.[11] Spindle-shaped cellulose nanocrystals

Dr. T. D. Nguyen, Dr. J. A. Kelly, Prof. M. J. MacLachlan
Department of Chemistry
University of British Columbia
2036 Main Mall, Vancouver
British Columbia V6T 1Z1, Canada
E-mail: mmaclach@chem.ubc.ca
Dr. W. Y. Hamad
FPInnovations
2665 East Mall
Vancouver, British Columbia, V6T 1Z4, Canada

DOI: 10.1002/adfm.201404304

(CNCs) prepared from bulk cellulose can self-assemble into a left-handed chiral nematic LC phase with structural colors.[12] Our group has recently reported a family of mesoporous materials exhibiting chiral nematic order using the self-assembly of CNCs.[13] For example, mixing a suitable silica precursor (e.g., $Si(OCH_3)_4$) in the presence of the lyotropic CNC dispersion produces a composite material in which SiO_2 uniformly cocondenses with CNCs exhibiting chiral nematic organization. Removal of the CNC template in the composites recovers mesoporous silica replicas.[13a] On the other hand, pyrolysis of the composites under N_2 converts CNCs to amorphous carbon, yielding uniform silica/carbon composites.[13b] The silica/carbon and mesoporous silica materials can be produced on a significant scale to give freestanding chiral nematic films with brilliant iridescence. Although the photonic properties of these CNC-templated materials could be useful in the form of porous semiconducting materials,[14] no precursors for these phases (e.g., Si or SiC) exist that are compatible with the self-assembly of aqueous CNC dispersions. As well, the small-sized mesopores of these materials are not compatible with the conventional CVD method to prepare photonic Si-based macroporous structures. Here, we have investigated the use of the magnesiothermic reaction to reduce silica/carbon and mesoporous silica films for preparing mesoporous SiC and Si replicas, respectively, with chiral nematic structures. We observe the formation of iridescent, mesoporous MgC_2/SiC mixtures as an intermediate from the magnesiothermic reduction of SiO_2/C. The synthesis, structural properties, and conductivity of these new materials are explored in detail.

2. Results and Discussion

2.1. Silicon Carbide from Magnesiothermic Reduction of Chiral Nematic Silica/Carbon

We found that the duration of the magnesiothermic reaction starting from the silica/carbon composites has a critical influence on the composition and long-range order of the resulting mesoporous SiC-based structures. The magnesiothermic reduction of the silica/carbon precursors was performed at 800 °C for 6, 12, or 24 h to generate crude product composites. These composites were then treated with dilute HCl for removal of MgO to obtain product composites denoted as **C-1**, **C-2**, and **C-3**, respectively. These samples were further purified by calcination and hydrogen fluoride (HF) etching to obtain samples **SC-1**, **SC-2**, and **SC-3**. At the early stages of the reaction (≤6 h), we observed the formation of dark-blue Mg_2Si by powder X-ray diffraction (PXRD, Figure S2, Supporting Information).[8b] Mg_2Si is a metastable intermediate that rapidly decomposes in water, leading to noticeable deterioration of the films during acid washing to remove MgO. Thus, **C-1** could not be purified to yield intact SiC-based films.

After 12 h of the magnesiothermic reduction treatment of silica/carbon, sample **C-2** was obtained as a robust film with slight iridescence (qualitatively indicating that the chiral nematic structure in the composites was retained during the reaction) (Figure S3a, Supporting Information). Unlike **C-1**, the films remained intact and iridescent throughout the purification steps, including treatment with 2 M HCl to remove MgO and calcination in air at 700 °C to burn out any remaining carbon. Subsequent removal of residual silica was accomplished by immersing the films in dilute HF. The green iridescence of the films of **SC-2** (**Figure 1**a, top) looks quite similar to jewel beetle shells (Figure 1b). The structural colors arise from chiral nematic ordering with a characteristic pitch on the order of the wavelengths of visible light. Conversely, after 24 h of reduction, the films of **SC-3** obtained after purification are brittle and brownish and show no iridescence (**Figure 2**b). To understand the compositional and morphological changes through this transformation, we characterized the product composites after removal of MgO (**C-2**, **C-3**) and purified products (**SC-2**, **SC-3**) with respect to their structural properties.

PXRD patterns (Figure 1c) of **C-2** and **SC-2** show broad reflections at 36°, 42°, and 62° 2θ that index to a tetragonal MgC_2-based structure.[15] This is in contrast to results from Dasog et al.[10] who observed the formation of Mg_2C_3 as an intermediate in the magnesiothermic reduction of silica/carbon mixtures. From Scherrer analysis of the width of the reflection peak at 42° 2θ, we estimate that the size of MgC_2-based crystallites (**SC-2**) is ≈6 nm. However, after 24 h of reduction, PXRD patterns (Figure 2c) of **C-3** and **SC-3** indicate the transformation of the tetragonal intermediate into a cubic β-SiC with a crystallite size of ≈4 nm estimated from the (111) diffraction peak.[8] After purification, **SC-3** exhibits enhanced intensity of the diffraction peaks relative to the amorphous background compared to **SC-2**, suggesting that a larger amount of impurities was removed. A trace Si phase formed in **C-3** during extended magnesiothermic reduction was oxidized to SiO_2 by the calcination step necessary for removal of free carbon. The residual silica component in the resulting samples was then etched away with dilute HF to obtain **SC-3** that shows the disappearance of the Si XRD features (Figure 2c).[6] Structural analysis of the products by Raman spectroscopy confirms a sharp peak at 796 cm^{-1} assigned to the Si-C stretching mode of SiC in **SC-3**,[16] whereas this peak is absent in **SC-2**, indicating a noticeable difference in the structures generated upon magnesiothermic reduction (Figure S6, Supporting Information).

Energy-dispersive X-ray (EDX) analyses averaged over different locations of the films show significant differences in the proportion of Mg in the samples prepared upon extended heating in the magnesiothermic reduction. About 6 wt% Mg was detected in **C-2** (Figure S4c, Supporting Information), whereas **C-3** contained only a trace amount of 0.4 wt% Mg (Figure S5c, Supporting Information). After purification, **SC-2** shows a small change in Mg composition (≈5 wt%) with 50 wt% Si, and 34 wt% C (Figure 1d), while **SC-3** contained 57 wt% Si, 31 wt% C, and no Mg (Figure 2d). About 8 wt% oxygen was detected in both **SC-2** and **SC-3**, which we attribute to a small amount of surface oxide species. Fourier transform IR spectra (Figure S4d,e, Supporting Information) of both **SC-2** and **SC-3** show a strong Si-C stretching mode at ≈800 cm^{-1} and the absence of Si–O–Si stretching modes at ≈1100 cm^{-1} for SiO_2. The thermal stability of the prepared samples was investigated by thermogravimetric analysis (TGA, Figures S4a and S5b, Supporting Information). The amount of free carbon in **C-2** (≈15 wt%) is much lower than that in **C-3** (≈35 wt%), indicating that a substantial amount of free carbon in the composites

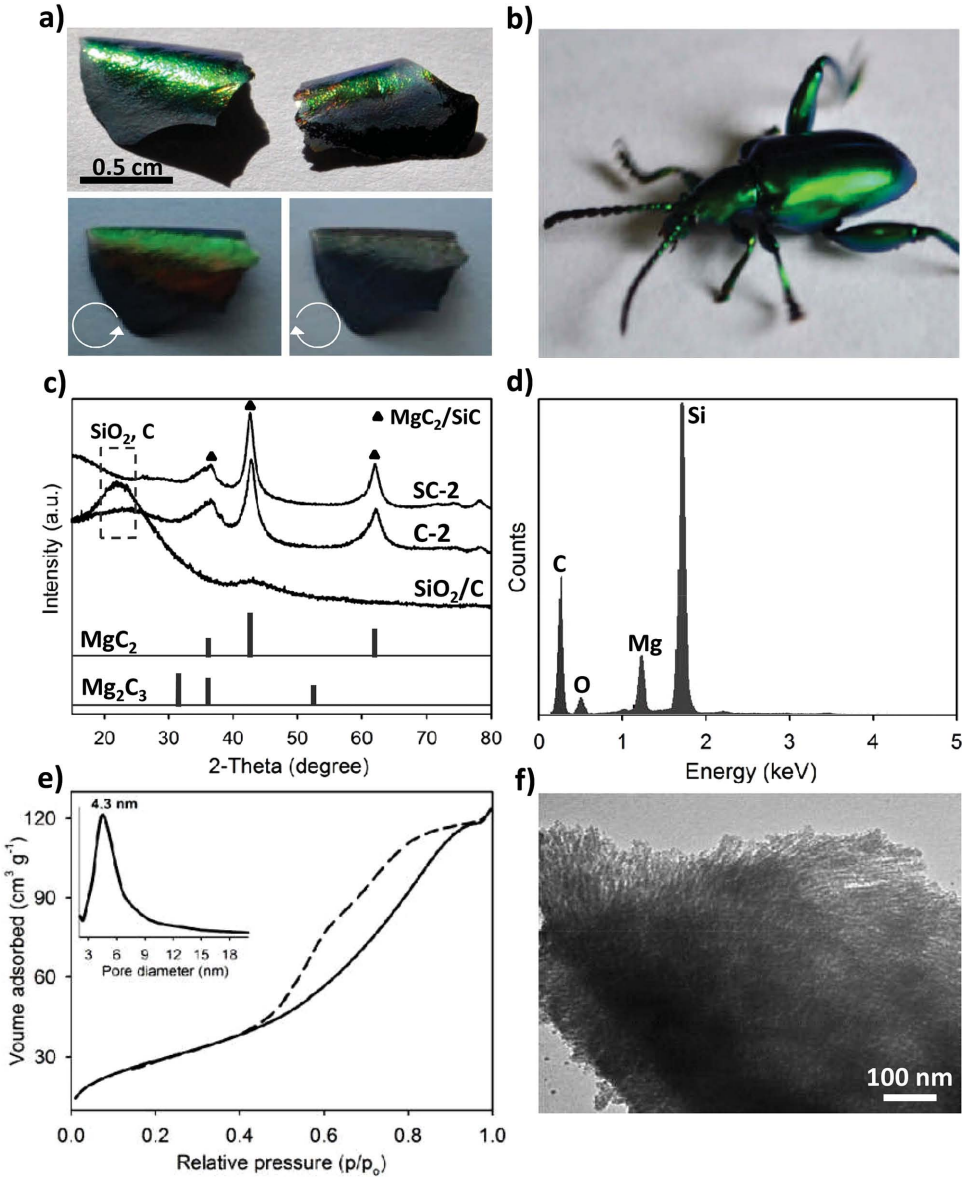

Figure 1. Chiral nematic mesoporous MgC_2/SiC mixtures. a) Photograph of MgC_2/SiC films (**SC-2**) showing green iridescence (top); the film observed under left- and right-handed circular polarizers (bottom). b) Photograph of a jewel beetle (credit: T.-D.N.). c) PXRD patterns of SiO_2/C, **C-2**, and **SC-2**. d) EDX spectrum, e) N_2 adsorption–desorption isotherms, inset showing a BJH pore size distribution, and f) TEM image of **SC-2**.

could react with Mg vapor to form MgC_2 then combine with SiC. The MgC_2/SiC mixtures were stable up to 900 °C in air while the oxidation of SiC to SiO_2 occurred at ≈700 °C.

Together, these characterization techniques indicate that the structure of the products obtained from the magnesiothermic reduction of the chiral nematic silica/carbon is strongly dependent upon the duration of heating. The comparative diffractogram results of MgC_2/SiC (**SC-2**) and MgC_2 reported in the literature[10] show that no significant shift of the PXRD peak positions was observed in both these samples (Figure 1c). We additionally performed the same magnesiothermic reaction with pure CNC films and carbonized CNC precursors, but no magnesium carbide compounds formed in amorphous carbons (Figure S7a, Supporting Information). Conversely, we found that a tetragonal MgC_2/SiC mixture rapidly forms in the silica/carbon composites either using very low silica loading or direct reduction of silica/CNC composites (Figure S7b, Supporting Information). These control experiments support a multistage formation pathway to SiC. It appears that the reduction of SiO_2/C by excess Mg is a fast exothermic reaction that first generates metastable Mg_2Si and then reacts further with carbon in the composites to form a mixture of silicon, magnesium and carbide species. Since two types of crystalline magnesium carbides, MgC_2 and Mg_2C_3, are known, it is sensible that the solid intermediates contain MgC_2 crystallites, which might preferentially form instead of Mg_2C_3[10] due to the difference in composition of the silica/CNC precursor and Mg vapor pressure in the reactor. These intermediates finally transform to SiC upon

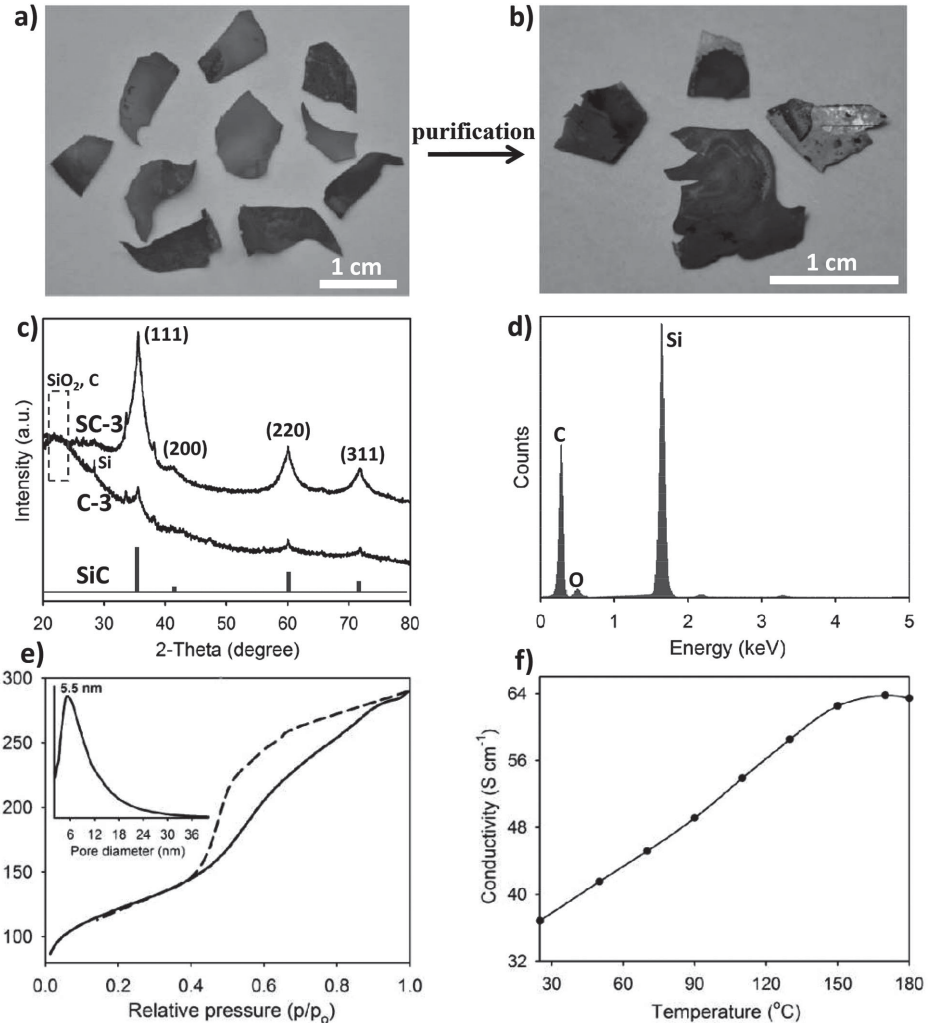

Figure 2. Mesoporous SiC replicas. Photographs of **C-3** a) before and b) after purification. c) PXRD patterns of **C-3** and **SC-3**. d) EDX spectrum, e) N_2 adsorption–desorption isotherms; inset showing a corresponding BJH pore size distribution, and f) temperature dependence of the conductivity of **SC-3**.

extended heating at 800 °C. Despite the fact that pure magnesium carbides are highly reactive upon exposure to water or water vapor,[15] we found that the **C-2** and **SC-2** samples were quite stable, with the MgC_2 phase still observed by PXRD even after high-temperature calcination in air. However, upon the magnesiothermic reduction, MgC_2 in the intermediate mixture that is a thermodynamically metastable structure reacted with Si to produce SiC when heating was extended.

Nitrogen sorption measurements of both **SC-2** (Figure 1e) and **SC-3** (Figure 2e) show a type-IV isotherm with type-H2 hysteresis characteristic of mesoporosity, whereas the reaction products **C-1** to **C-3** do not show any porosity (data not shown). This suggests that the removal of residual carbon and silica from the product composites leads to an opening of the structure, leading to porosity. The Brunauer–Emmett–Teller (BET) surface area and pore volumes were estimated to be 106 $m^2\ g^{-1}$ and 0.20 $cm^3\ g^{-1}$ for MgC_2/SiC (**SC-2**) and 400 $m^2\ g^{-1}$ and 0.36 $cm^3\ g^{-1}$ for SiC (**SC-3**), respectively. The Barrett–Joyner–Halenda (BJH) pore size distribution of **SC-2** is about 3–7 nm, which is smaller than the 4–12 nm pore diameters of **SC-3**. The lower surface area of the MgC_2/SiC films may result from the thicker walls. An increase in the surface area, pore volume, and pore size upon extended heating to form SiC compared to MgC_2/SiC is consistent with the removal of remaining Mg-containing species in the films after complete transformation, leaving behind additional pores in the SiC mesostructures. However, the SiC-based films have lower surface area and higher microporosity (≈85 $m^2\ g^{-1}$) than those of the chiral nematic mesoporous silica.[13a] Transmission electron microscopy (TEM) images support the presence of long-range porosity within the MgC_2/SiC films (Figure 1f), resembling TEM images of chiral nematic mesoporous silica.[13b] The SiC films show a loss of order, with the observation of aggregated grains in a chain-like porous structure with a lower degree of interconnectivity (Figure S9a, Supporting Information).

Scanning electron microscopy (SEM) confirms the retention of the chiral nematic structure throughout the transformation (**Figures 3** and S8, Supporting Information). A repeating layered structure is observed at fracture cross sections of the films for both MgC_2/SiC (**SC-2**) and SiC (**SC-3**). Closely resembling

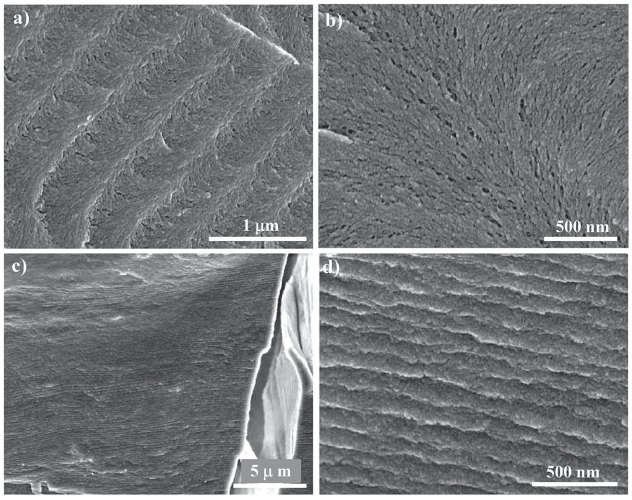

Figure 3. Chiral nematic organization of mesoporous mixed MgC_2/SiC and SiC materials. SEM images viewed along a) fracture cross sections and b) flat top surfaces of the MgC_2/SiC films (**SC-2**). c,d) SEM images viewed along fracture cross sections of the SiC films (**SC-3**) at different scales.

the parent chiral nematic silica/carbon films[17] and in keeping with their intense iridescence, the MgC_2/SiC films show twisted spindle-like features rotated in a counter-clockwise direction at fracture edges. The surface is relatively flat, with a texture of nanospindles parallel to each other. The SiC films basically retain the overall layered structure of the parent composites, but with some loss of order, small cracks, and a rougher surface. As well, at the nanostructure, the SiC films appear as globular crystalline particles rather than the spindle-like morphology observed in the MgC_2/SiC mixtures. We postulate that the diminished structural order of the mesoporous SiC results from the phase transformation accompanied by releasing Mg species in the intermediates.

The MgC_2/SiC films (**SC-2**) still retain their iridescence and crystallinity even after sequential treatment with etching agents and high-temperature heating (at 900 °C in air), demonstrating their excellent chemical inertness and corrosion resistance. The MgC_2/SiC films were photographed using left-handed and right-handed circular polarizing filters (LHP and RHP, respectively). The films appear green under a LHP filter and dull under a RHP filter (Figure 1a, bottom). This is further proof for replication of the parent left-handed chiral nematic structure templated from CNCs, as chiral nematic structures selectively reflect circularly polarized light with a handedness that matches that of the structure. The MgC_2/SiC films soaked with water show a drastic reduction of the iridescent colors resulting from filling water in the pores, leading to near refractive index matching between water in the pores and MgC_2/SiC walls (Figure S3b, Supporting Information). However, the optical properties of the films could not be characterized by conventional optical techniques such as polarized optical microscopy and circular dichroism because of the opacity of the material. The SiC films show only slightly birefringent textures under crossed polarizers suggestive of some loss of chiral nematic order (Figure S9b, Supporting Information). We investigated the temperature dependence of the conductivity of the SiC films (**SC-3**) measured by a four-probe method. Figure 2f shows that the conductivity increases from 37 to 64 S cm^{-1} within the range of 25–170 °C, indicating semiconducting behavior.

2.2. Silicon from Magnesiothermic Reduction of Chiral Nematic Mesoporous Silica

By performing the magnesiothermic reduction using mesoporous silica (obtained from calcining chiral nematic SiO_2/CNC composites in air; characterization given in Figure S10, Supporting Information), we sought to adapt this method to produce mesoporous Si replicas. Reduction of the silica films by hot Mg vapor (1.0:2.5 SiO_2:Mg mass ratio) at 800 °C yielded crude product composites containing Si and by-products. As with the reduction of silica/carbon, we found that the long-range periodic order of the resulting porous Si structure is strongly dependent upon the duration of heating. We carried out the magnesiothermic reactions for three different periods (6, 12, or 24 h) to yield product composites denoted as **S-1**, **S-2**, and **S-3**. Subsequent purification by acid extraction of impurities gave Si samples **SI-1**, **SI-2**, and **SI-3**, respectively.

The films obtained after the magnesiothermic reaction show a change in color from dark blue to black-brown and dull brown upon extended heating from 6 to 12 and 24 h (Figure S11, Supporting Information). As in the SiC preparation, **S-1** could not be purified to yield intact Si films because of the generation of the metastable Mg_2Si intermediates in the early reaction steps (Figure S12a, Supporting Information).[6] The PXRD pattern of **S-2** shows that it is a mixture of three different phases: Si, MgO, and trace Mg_2Si (Figure S12b, Supporting Information). Electron microscopy confirmed the retention of chiral nematic order in **S-2** under these reaction conditions (**Figure 4**b). Iridescent, pale-yellow, brittle Si films (**SI-2**) were obtained by sequentially treating the reaction products with 2 M HCl and 2% HF to remove Mg_2Si/MgO and surface oxide species, respectively (Figure 4a). **SI-2** basically retains the long-range layered structure of the parent silica but with additional large voids within the films (Figure 4c). The PXRD pattern of **SI-2** (Figure 4d) shows sharp peaks indexed to a pure diamond-lattice Si crystal, consistent with the removal of Mg_2Si/MgO impurities.[6] Compared with the diffractograms of SiC, the Si samples exhibit very sharp and intense diffraction peaks indicative of larger crystallites, with an estimated crystallite size of ≈26 nm (Scherrer analysis from the (111) reflection). An EDX spectrum of **SI-2** (Figure 4e) confirms that the material is entirely silicon; for comparison, an EDX spectrum of mesoporous silica films shows simultaneous detection of Si and O elements (Figure S13a, Supporting Information). Magnesium components were not detected in the final Si products.

The porosity of the Si films (**SI-2**) was studied by nitrogen sorption, which shows a type-IV isotherm with type-H3 hysteresis characteristic of slit-shaped mesopores and BET surface area of 150 m^2 g^{-1} (Figure S13d, Supporting Information). The surface area and pore volume noticeably decreased as a result of the growth of large-sized Si crystals within the films during the magnesiothermic reduction. The Si films (**SI-2**) are semiconducting and exhibit an increase in the electrical conductivity from 24 to 49 S cm^{-1} as the temperature is raised from 25 and

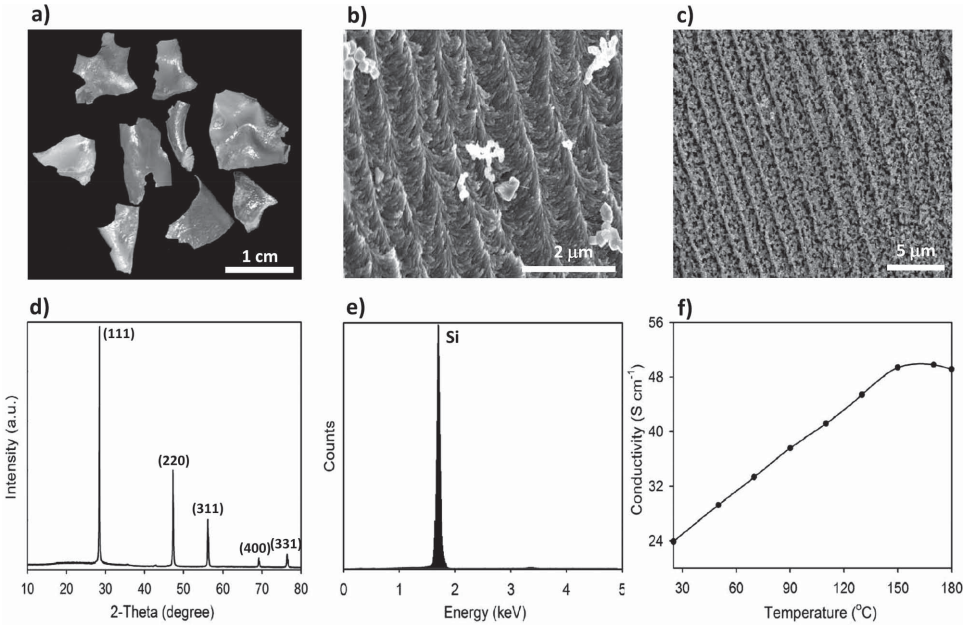

Figure 4. Mesoporous Si films prepared from the magnesiothermic reduction of chiral nematic mesoporous silica. a) Photograph of Si films (**SI-2**). SEM images of b) the product composites (**S-2**) and c) **SI-2** viewed along fracture cross sections. d) PXRD pattern, e) EDX spectrum, and f) variable temperature conductivity plot of **SI-2**.

150 °C (Figure 4f); impurities in the Si must be responsible for its relatively high conductivity. We postulate that the mesostructure of the parent silica films facilitates diffusion of Mg vapors during vapor-phase magnesiothermic reaction, leading to the growth of large MgO crystals inside the pores. Removal of the MgO crystals in the acid wash procedure leaves behind large voids and partial destruction of chiral nematic order. As the heating time is extended (**SI-3**), long-range order is further disrupted by overgrowth of larger MgO crystals leading to near-complete destruction of chiral nematic order (Figure S14, Supporting Information). These results are consistent with other attempts to use magnesiothermic reduction to convert mesoporous SiO_2 to Si replicas, resulting in a loss of order.[7] These results suggest a lower size limit that can be successfully replicated in the pure Si structures through this process.

3. Conclusions

In summary, we have demonstrated, for the first time, the preparation of mesoporous SiC and Si using the reduction of chiral nematic silica/carbon and mesoporous silica derived from CNC assemblies. Magnesiothermic reduction of silica/carbon first forms metastable Mg_2Si and then transforms into MgC_2/SiC intermediates and finally to SiC upon extended heating at 800 °C within 24 h. After purification, iridescent, black mesoporous MgC_2/SiC structures with chiral nematic ordering were obtained from the intermediates. Pale-yellow mesoporous SiC replicas with diminished chiral nematic ordering were recovered from the final composite products. It is worth noting that the MgC_2/SiC intermediate samples, which exhibit excellent thermal stability and intense iridescence, appear to be unique to our system. The magnesiothermic reaction was applied to reduce the chiral nematic mesoporous silica for creating mesoporous Si crystalline films with a layered structure. These novel crystalline, semiconducting SiC and Si mesoporous materials may be useful in sensing and other applications.

4. Experimental Section

Reagents and characterization details are provided in Supporting Information.

Preparation of Chiral Nematic Silica/Carbon and Mesoporous Silica: Chiral nematic silica/carbon and mesoporous silica films with appropriate $Si(OCH_3)_4$/CNC ratios were prepared according to previous studies.[13a,b] In general, we found that the silica/carbon composites with a low silica loading (e.g., 0.15 mL $Si(OCH_3)_4$ mixed with 5.0 mL of 3.0 wt% CNC dispersion, ≤30 wt% silica in composites estimated by TGA, Figure S1d, Supporting Information) are better precursors for converting to SiC with minimal generation of Si. The silica/CNC composites were first carbonized by heating under flowing N_2 to 900 °C (Figure S1b, Supporting Information). Intact mesoporous Si films were best obtained from mesoporous silica films with thick walls that were prepared from cocondensing 0.23 mL $Si(OCH_3)_4$ with 5.0 mL of 3.0 wt% CNC dispersion followed by calcining at 540 °C in air (Figure S10, Supporting Information).

Magnesiothermic Reduction of Silica/Carbon: Silica/carbon precursors (140 mg) and metallic Mg turnings (350 mg) were placed at opposite ends of a rectangle-shaped stainless steel boat (width 1 cm, length 15 cm, height 1.2 cm). Excess Mg was used to guarantee the complete reduction of silica. The boat was tightly sealed with a cap and inserted into a stainless steel tube furnace (diameter 2.5 cm, length 100 cm). The reaction mixture was heated under flowing argon (50 mL min^{-1}) to 800 °C at a rate of 5 °C min^{-1} and held at this temperature for different reaction times ranging from 6 to 24 h. After cooling to room temperature, the composite films were treated with 2 M HCl at room temperature for 4 h to dissolve MgO by-product. The films were then calcined at 700 °C in air for 6 h to eliminate residual carbon. The films were then etched in 2% HF aqueous solution to remove residual silica

and finally vacuum-dried at 60 °C for 8 h. After purification, black films were obtained after 12 h of heating, which transformed to pale-yellow upon extended heating for 24 h. Typical yields after these purification steps were ≈68% after 12 h reduction and ≈29% after 24 h reduction.

Magnesiothermic Reduction of Mesoporous Silica: The reduction was carried out as described above using 140 mg of chiral nematic mesoporous SiO_2 films. The resulting films were treated with 2 M HCl and 2% HF as described above. A typical reaction yield was ≈43%.

Supporting Information

Supporting Information is available from the Wiley Online Library or from the author.

Acknowledgements

The authors acknowledge financial support from the Natural Sciences and Engineering Research Council (NSERC) and are thankful to CelluForce Inc. for providing CNCs. T.-D.N. and J.A.K. are both grateful to NSERC for Postdoctoral Fellowships.

Received: December 04, 2014
Revised: January 21, 2015
Published online: February 25, 2015

[1] a) G. S. Armatas, M. G. Kanatzidis, *Nature* **2006**, *441*, 1122; b) S. Bag, P. N. Trikalitis, P. J. Chupas, G. S. Armatas, M. G. Kanatzidis, *Science* **2007**, *317*, 490; c) P. McCord, S. L. Yau, A. J. Bard, *Science* **1992**, *257*, 68; d) K. Aoki, H. T. Miyazaki, H. Hirayama, K. Inoshita, T. Baba, K. Sakoda, N. Shinya, Y. Aoyagi, *Nat. Mater.* **2003**, *2*, 117.

[2] a) B. K. Teo, X. H. Sun, *Chem. Rev.* **2007**, *107*, 1454; b) T. S aga, *NPG Asia Mater.* **2010**, *2*, 96; c) A. I. Hochbaum, P. Yang, *Chem. Rev.* **2010**, *110*, 527; d) H. Pedersen, S. Leone, O. Kordina, A. Henr, S. Nishizawa, Y. Koshka, E. Janzen, *Chem. Rev.* **2012**, *112*, 2434; e) L. Borchardt, C. Hoffmann, M. Oschatz, L. Mammitzsch, U. Petasch, M. Herrmann, S. Kaskel, *Chem. Soc. Rev.* **2012**, *41*, 5053; f) M. L. Snedaker, Y. Zhang, C. S. Birkel, H. Wang, T. Day, Y. Shi, X. Ji, S. Kraemer, C. E. Mills, A. Moosazadeh, M. Moskovits, G. J. Snyder, G. D. Stucky, *Chem. Mater.* **2013**, *25*, 4867; g) M. Amato, M. Palummo, R. Rurali, S. Ossicini, *Chem. Rev.* **2014**, *114*, 1371; h) H. Jia, R. Kloepsch, X. He, J. P. Badillo, P. Gao, O. Fromm, T. Placke, M. Winter, *Chem. Mater.* **2014**, *26*, 5683.

[3] a) M. P. Stewart, J. M. Buriak, *Adv. Mater.* **2000**, *12*, 859; b) J. G. C. Veinot, *Chem. Commun.* **2006**, 4160; c) J. H. Park, L. Gu, G. Maltzahn, E. Ruoslahti, S. N. Bhatia, M. J. Sailor, *Nat. Mater.* **2009**, *8*, 331; d) J. A. Kelly, E. J. Henderson, J. G. C. Veinot, *Chem. Commun.* **2010**, *46*, 8704.

[4] a) N. Tetreault, H. Miguez, G. A. Ozin, *Adv. Mater.* **2004**, *16*, 1471; b) X. Chen, C. Li, H. K. Tsang, *NPG Asia Mater.* **2011**, *3*, 34; c) H. Hu, J. Tang, H. Zhong, Z. Xi, C. Chen, Q. Chen, *Sci. Rep.* **2013**, *3*, 1484; d) Z. Xia, S. C. Davis, A. A. Eftekhar, A. S. Gordin, M. Askari, Q. Li, F. Ghasemi, K. H. Sandhage, A. Adibi, *Adv. Opt. Mater.* **2014**, *2*, 235.

[5] a) J. Zhou, H. Li, L. Ye, J. Liu, J. Wang, T. Zhao, L. Jiang, Y. Song, *J. Phys. Chem. C* **2010**, *114*, 22303; b) A. Blanco, E. Chomski, S. Grabtchak, M. Ibisate, S. John, S. W. Leonard, C. Lopez, F. Meseguer, H. Miguez, J. P. Mondia, G. A. Ozin, O. Toader, H. M. Driel, *Nature* **2000**, *405*, 437.

[6] Z. Bao, M. R. Weatherspoon, S. Shian, Y. Cai, P. D. Graham, S. M. Allan, G. Ahmad, M. B. Dickerson, B. C. Church, Z. Kang, H. W. Abernathy III, C. J. Summers, M. Liu, K. H. Sandhage, *Nature* **2007**, *446*, 172.

[7] a) M. Ibisate, D. Golmayo, C. Lopez, *Adv. Mater.* **2009**, *21*, 2899; b) E. K. Richman, C. B. Kang, T. Brezesinski, S. H. Tolbert, *Nano Lett.* **2008**, *8*, 3075; c) W. Luo, X. Wang, C. Meyers, N. Wannenmacher, W. Sirisaksoontorn, M. M. Lerner, X. Ji, *Sci. Rep.* **2013**, *3*, 2222; d) N. Liu, K. Huo, M. T. McDowell, J. Zhao, Y. Cui. *Sci. Rep.* **2013**, *3*, 1919; e) J. K. Yoo, J. Kim, M. J. Choi, Y. U. Park, J. Hong, K. M. Baek, K. Kang, Y. S. Jung, *Adv. Energy Mater.* **2014**, *4*, 1400622.

[8] a) Y. Shi, F. Zhang, Y. S. Hu, X. Sun, Y. Zhang, H. I. Lee, L. Chen, G. D. Stucky, *J. Am. Chem. Soc.* **2010**, *132*, 5552; b) P. C. Gao, Y. Lei, A. F. C. Perez, K. Rajoua, D. Zitoun, F. Favier, J. *Mater. Chem.* **2011**, *21*, 15798.

[9] Y. F. Shi, Y. Meng, D. H. Chen, S. J. Cheng, P. Chen, H. F. Yang, Y. Wan, D. Y. Zhao, *Adv. Funct. Mater.* **2006**, *16*, 561.

[10] M. Dasog, L. F. Smith, T. K. Purkait, J. G. C. Veinot, *Chem. Commun.* **2013**, *49*, 7004.

[11] a) M. O'Neill, S. M. Kelly, *Adv. Mater.* **2003**, *15*, 1135; b) E. K. Fleischmann, R. Zentel, *Angew. Chem. Int. Ed.* **2013**, *52*, 8810.

[12] a) R. H. Marchessault, F. F. Morehead, N. M. Walter, *Nature* **1959**, *184*, 632; b) J. F. Revol, L. Godbout, D. G. Gray, *J. Pulp Pap. Sci.* **1998**, *24*, 146; c) W. Y. Hamad, T. Q. Hu, *Can. J. Chem. Eng.* **2010**, *88*, 392; d) S. Beck, J. Bouchard, G. Chauve, R. Berry, *Cellulose* **2013**, *20*, 1401; e) J. P. F. Lagerwall, C. Schutz, M. Salajkova, J. Noh, J. H. Park, G. Scalia, L. Bergstrom, *NPG Asia Mater.* **2014**, *6*, e80.

[13] a) K. E. Shopsowitz, H. Qi, W. Y. Hamad, M. J. MacLachlan, *Nature* **2010**, *468*, 422; b) K. E. Shopsowitz, W. Y. Hamad, M. J. MacLachlan, *Angew. Chem. Int. Ed.* **2011**, *50*, 10991; c) J. A. Kelly, M. Giese, K. E. Shopsowitz, W. Y. Hamad, M. J. MacLachlan, *Acc. Chem. Res.* **2014**, *47*, 1088.

[14] T. D. Nguyen, W. Y. Hamad, M. J. MacLachlan, *Adv. Funct. Mater.* **2014**, *24*, 777.

[15] a) H. Fjellvag, P. Karen, *Inorg. Chem.* **1992**, *31*, 3260; b) P. Redondo, C. Barrientos, A. Cimas, A. Largo, *J. Phys. Chem. A* **2003**, *107*, 6317; c) O. O. Kurakevych, T. A. Strobel, D. Y. Kim, G. D. Cody, *Angew. Chem. Int. Ed.* **2013**, *52*, 8930; d) T. A. Strobel, O. O. Kurakevych, D. Y. Kim, Y. L. Godec, W. Crichton, J. Guignard, N. Guignot, G. D. Cody, A. R. Oganov, *Inorg. Chem.* **2014**, *53*, 7020.

[16] J. Frechette, C. Carraro, *J. Am. Chem. Soc.* **2006**, *128*, 14774.

[17] T. D. Nguyen, W. Y. Hamad, M. J. MacLachlan, *Chem. Commun.* **2013**, *49*, 11296.